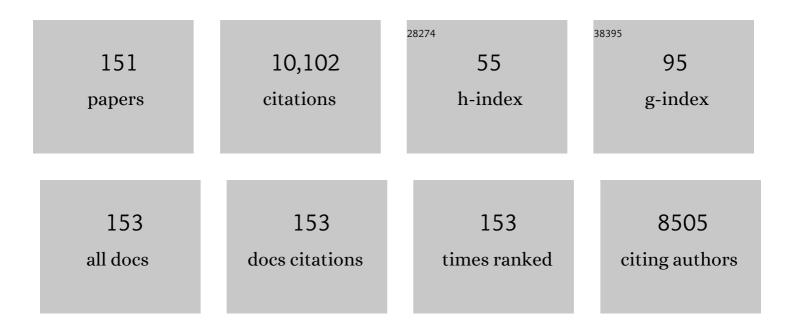
## Jingwei Dong

List of Publications by Year in descending order

Source: https://exaly.com/author-pdf/329042/publications.pdf Version: 2024-02-01



LINCWEL DONC

#	Article	IF	CITATIONS
1	Green-up dates in the Tibetan Plateau have continuously advanced from 1982 to 2011. Proceedings of the United States of America, 2013, 110, 4309-4314.	7.1	528
2	Mapping paddy rice planting area in northeastern Asia with Landsat 8 images, phenology-based algorithm and Google Earth Engine. Remote Sensing of Environment, 2016, 185, 142-154.	11.0	524
3	A global moderate resolution dataset of gross primary production of vegetation for 2000–2016. Scientific Data, 2017, 4, 170165.	5.3	335
4	The rapid and massive urban and industrial land expansions in China between 1990 and 2010: A CLUD-based analysis of their trajectories, patterns, and drivers. Landscape and Urban Planning, 2016, 145, 21-33.	7.5	314
5	A mangrove forest map of China in 2015: Analysis of time series Landsat 7/8 and Sentinel-1A imagery in Google Earth Engine cloud computing platform. ISPRS Journal of Photogrammetry and Remote Sensing, 2017, 131, 104-120.	11.1	288
6	Joint control of terrestrial gross primary productivity by plant phenology and physiology. Proceedings of the National Academy of Sciences of the United States of America, 2015, 112, 2788-2793.	7.1	265
7	Tracking the dynamics of paddy rice planting area in 1986–2010 through time series Landsat images and phenology-based algorithms. Remote Sensing of Environment, 2015, 160, 99-113.	11.0	257
8	Observations and Modeling of the Climatic Impact of Land-Use Changes 2014. Advances in Meteorology, 2015, 2015, 1-2.	1.6	213
9	Mapping paddy rice planting areas through time series analysis of MODIS land surface temperature and vegetation index data. ISPRS Journal of Photogrammetry and Remote Sensing, 2015, 106, 157-171.	11.1	207
10	Divergent trends of open-surface water body area in the contiguous United States from 1984 to 2016. Proceedings of the National Academy of Sciences of the United States of America, 2018, 115, 3810-3815.	7.1	199
11	Mapping deciduous rubber plantations through integration of PALSAR and multi-temporal Landsat imagery. Remote Sensing of Environment, 2013, 134, 392-402.	11.0	183
12	Evolution of regional to global paddy rice mapping methods: A review. ISPRS Journal of Photogrammetry and Remote Sensing, 2016, 119, 214-227.	11.1	181
13	Consistency between sun-induced chlorophyll fluorescence and gross primary production of vegetation in North America. Remote Sensing of Environment, 2016, 183, 154-169.	11.0	180
14	Ten facts about land systems for sustainability. Proceedings of the National Academy of Sciences of the United States of America, 2022, 119, .	7.1	157
15	Effectiveness of ecological restoration projects in Horqin Sandy Land, China based on SPOT-VGT NDVI data. Ecological Engineering, 2012, 38, 20-29.	3.6	151
16	Examining earliest identifiable timing of crops using all available Sentinel 1/2 imagery and Google Earth Engine. ISPRS Journal of Photogrammetry and Remote Sensing, 2020, 161, 109-123.	11.1	148
17	Open Surface Water Mapping Algorithms: A Comparison of Water-Related Spectral Indices and Sensors. Water (Switzerland), 2017, 9, 256.	2.7	147
18	Tracking annual changes of coastal tidal flats in China during 1986–2016 through analyses of Landsat images with Google Earth Engine. Remote Sensing of Environment, 2020, 238, 110987.	11.0	146

#	Article	IF	CITATIONS
19	The 10-m crop type maps in Northeast China during 2017–2019. Scientific Data, 2021, 8, 41.	5.3	141
20	Mapping coastal wetlands of China using time series Landsat images in 2018 and Google Earth Engine. ISPRS Journal of Photogrammetry and Remote Sensing, 2020, 163, 312-326.	11.1	138
21	Spatiotemporal patterns of paddy rice croplands in China and India from 2000 to 2015. Science of the Total Environment, 2017, 579, 82-92.	8.0	127
22	Mapping paddy rice planting area in cold temperate climate region through analysis of time series Landsat 8 (OLI), Landsat 7 (ETM+) and MODIS imagery. ISPRS Journal of Photogrammetry and Remote Sensing, 2015, 105, 220-233.	11.1	118
23	Continued decrease of open surface water body area in Oklahoma during 1984–2015. Science of the Total Environment, 2017, 595, 451-460.	8.0	118
24	Continuous monitoring of lake dynamics on the Mongolian Plateau using all available Landsat imagery and Google Earth Engine. Science of the Total Environment, 2019, 689, 366-380.	8.0	116
25	Mapping tropical forests and rubber plantations in complex landscapes by integrating PALSAR and MODIS imagery. ISPRS Journal of Photogrammetry and Remote Sensing, 2012, 74, 20-33.	11.1	107
26	High resolution paddy rice maps in cloud-prone Bangladesh and Northeast India using Sentinel-1 data. Scientific Data, 2019, 6, 26.	5.3	107
27	Mapping sugarcane plantation dynamics in Guangxi, China, by time series Sentinel-1, Sentinel-2 and Landsat images. Remote Sensing of Environment, 2020, 247, 111951.	11.0	105
28	Large increases of paddy rice area, gross primary production, and grain production in Northeast China during 2000–2017. Science of the Total Environment, 2020, 711, 135183.	8.0	104
29	Sensitivity of vegetation indices and gross primary production of tallgrass prairie to severe drought. Remote Sensing of Environment, 2014, 152, 1-14.	11.0	103
30	Mapping paddy rice planting area in rice-wetland coexistent areas through analysis of Landsat 8 OLI and MODIS images. International Journal of Applied Earth Observation and Geoinformation, 2016, 46, 1-12.	2.8	103
31	Rebound in China's coastal wetlands following conservation and restoration. Nature Sustainability, 2021, 4, 1076-1083.	23.7	103
32	Comparison of four EVI-based models for estimating gross primary production of maize and soybean croplands and tallgrass prairie under severe drought. Remote Sensing of Environment, 2015, 162, 154-168.	11.0	93
33	A comparison of forest cover maps in Mainland Southeast Asia from multiple sources: PALSAR, MERIS, MODIS and FRA. Remote Sensing of Environment, 2012, 127, 60-73.	11.0	91
34	Mapping Deciduous Rubber Plantation Areas and Stand Ages with PALSAR and Landsat Images. Remote Sensing, 2015, 7, 1048-1073.	4.0	89
35	Identifying floods and flood-affected paddy rice fields in Bangladesh based on Sentinel-1 imagery and Google Earth Engine. ISPRS Journal of Photogrammetry and Remote Sensing, 2020, 166, 278-293.	11.1	89
36	Elevation-dependent relationships between climate change and grassland vegetation variation across the Qinghai-Xizang Plateau. International Journal of Climatology, 2015, 35, 1638-1647.	3.5	85

#	Article	IF	CITATIONS
37	Divergent shifts in peak photosynthesis timing of temperate and alpine grasslands in China. Remote Sensing of Environment, 2019, 233, 111395.	11.0	85
38	Exacerbated grassland degradation and desertification in Central Asia during 2000–2014. Ecological Applications, 2018, 28, 442-456.	3.8	83
39	Gainers and losers of surface and terrestrial water resources in China during 1989–2016. Nature Communications, 2020, 11, 3471.	12.8	81
40	Decreasing net primary production due to drought and slight decreases in solar radiation in China from 2000 to 2012. Journal of Geophysical Research G: Biogeosciences, 2017, 122, 261-278.	3.0	80
41	Influence of Urbanization Factors on Surface Urban Heat Island Intensity: A Comparison of Countries at Different Developmental Phases. Sustainability, 2016, 8, 706.	3.2	76
42	Elevationâ€dependent effects of climate change on vegetation greenness in the high mountains of southwest China during 1982–2013. International Journal of Climatology, 2018, 38, 2029-2038.	3.5	76
43	Social functional mapping of urban green space using remote sensing and social sensing data. ISPRS Journal of Photogrammetry and Remote Sensing, 2018, 146, 436-452.	11.1	73
44	Spatio-temporal changes in annual accumulated temperature in China and the effects on cropping systems, 1980s to 2000. Climate Research, 2009, 40, 37-48.	1.1	72
45	Improved estimates of forest cover and loss in the Brazilian Amazon in 2000–2017. Nature Sustainability, 2019, 2, 764-772.	23.7	71
46	Cropland redistribution to marginal lands undermines environmental sustainability. National Science Review, 2022, 9, nwab091.	9.5	71
47	Forest cover maps of China in 2010 from multiple approaches and data sources: PALSAR, Landsat, MODIS, FRA, and NFI. ISPRS Journal of Photogrammetry and Remote Sensing, 2015, 109, 1-16.	11.1	70
48	Mapping tropical forests and deciduous rubber plantations in Hainan Island, China by integrating PALSAR 25-m and multi-temporal Landsat images. International Journal of Applied Earth Observation and Geoinformation, 2016, 50, 117-130.	2.8	69
49	Changes in area and number of nature reserves in China. Conservation Biology, 2019, 33, 1066-1075.	4.7	68
50	Mapping the dynamics of eastern redcedar encroachment into grasslands during 1984–2010 through PALSAR and time series Landsat images. Remote Sensing of Environment, 2017, 190, 233-246.	11.0	65
51	Northward expansion of paddy rice in northeastern Asia during 2000–2014. Geophysical Research Letters, 2016, 43, 3754-3761.	4.0	63
52	Land claim and loss of tidal flats in the Yangtze Estuary. Scientific Reports, 2016, 6, 24018.	3.3	62
53	Automatic land cover classification of geo-tagged field photos by deep learning. Environmental Modelling and Software, 2017, 91, 127-134.	4.5	62
54	Application of the water-related spectral reflectance indices: A review. Ecological Indicators, 2019, 98, 68-79.	6.3	62

#	Article	IF	CITATIONS
55	Evolution of light use efficiency models: Improvement, uncertainties, and implications. Agricultural and Forest Meteorology, 2022, 317, 108905.	4.8	62
56	Characterizing the encroachment of juniper forests into sub-humid and semi-arid prairies from 1984 to 2010 using PALSAR and Landsat data. Remote Sensing of Environment, 2018, 205, 166-179.	11.0	61
57	Comparison of Gross Primary Productivity Derived from GIMMS NDVI3g, GIMMS, and MODIS in Southeast Asia. Remote Sensing, 2014, 6, 2108-2133.	4.0	59
58	Precipitation and carbon-water coupling jointly control the interannual variability of global land gross primary production. Scientific Reports, 2016, 6, 39748.	3.3	57
59	Fingerprint of rice paddies in spatial–temporal dynamics of atmospheric methane concentration in monsoon Asia. Nature Communications, 2020, 11, 554.	12.8	56
60	Mapping paddy rice planting area in wheat-rice double-cropped areas through integration of Landsat-8 OLI, MODIS and PALSAR images. Scientific Reports, 2015, 5, 10088.	3.3	55
61	Increasing cropping intensity in response to climate warming in Tibetan Plateau, China. Field Crops Research, 2013, 142, 36-46.	5.1	54
62	Comparison of three remotely sensed drought indices for assessing the impact of drought on winter wheat yield. International Journal of Digital Earth, 2020, 13, 504-526.	3.9	54
63	Mapping Oil Palm Plantations in Cameroon Using PALSAR 50-m Orthorectified Mosaic Images. Remote Sensing, 2015, 7, 1206-1224.	4.0	52
64	Global observation of urban expansion and land-cover dynamics using satellite big-data. Science Bulletin, 2021, 66, 297-300.	9.0	50
65	Mapping forests in monsoon Asia with ALOS PALSAR 50-m mosaic images and MODIS imagery in 2010. Scientific Reports, 2016, 6, 20880.	3.3	49
66	The 2012 Flash Drought Threatened US Midwest Agroecosystems. Chinese Geographical Science, 2019, 29, 768-783.	3.0	48
67	Annual dynamics of forest areas in South America during 2007–2010 at 50-m spatial resolution. Remote Sensing of Environment, 2017, 201, 73-87.	11.0	47
68	A 50-m Forest Cover Map in Southeast Asia from ALOS/PALSAR and Its Application on Forest Fragmentation Assessment. PLoS ONE, 2014, 9, e85801.	2.5	46
69	Spatio-temporal prediction of leaf area index of rubber plantation using HJ-1A/1B CCD images and recurrent neural network. ISPRS Journal of Photogrammetry and Remote Sensing, 2015, 102, 148-160.	11.1	46
70	Remote sensing and geospatial technologies in support of a normative land system science: status and prospects. Current Opinion in Environmental Sustainability, 2019, 38, 44-52.	6.3	45
71	Spatio-temporal pattern and rationality of land reclamation and cropland abandonment in mid-eastern Inner Mongolia of China in 1990–2005. Environmental Monitoring and Assessment, 2011, 179, 137-153.	2.7	42
72	Modeling gross primary production of paddy rice cropland through analyses of data from CO2 eddy flux tower sites and MODIS images. Remote Sensing of Environment, 2017, 190, 42-55.	11.0	42

#	Article	IF	CITATIONS
73	Quantifying annual changes in built-up area in complex urban-rural landscapes from analyses of PALSAR and Landsat images. ISPRS Journal of Photogrammetry and Remote Sensing, 2017, 124, 89-105.	11.1	42
74	Performance of four state-of-the-art GPP products (VPM, MOD17, BESS and PML) for grasslands in drought years. Ecological Informatics, 2020, 56, 101052.	5.2	42
75	Early- and in-season crop type mapping without current-year ground truth: Generating labels from historical information via a topology-based approach. Remote Sensing of Environment, 2022, 274, 112994.	11.0	42
76	Examining the short-term impacts of diverse management practices on plant phenology and carbon fluxes of Old World bluestems pasture. Agricultural and Forest Meteorology, 2017, 237-238, 60-70.	4.8	41
77	Quantifying agricultural drought in tallgrass prairie region in the U.S. Southern Great Plains through analysis of a water-related vegetation index from MODIS images. Agricultural and Forest Meteorology, 2017, 246, 111-122.	4.8	40
78	Has climate change driven spatio-temporal changes of cropland in northern China since the 1970s?. Climatic Change, 2014, 124, 163-177.	3.6	39
79	Mapping paddy rice distribution using multi-temporal Landsat imagery in the Sanjiang Plain, northeast China. Frontiers of Earth Science, 2016, 10, 49-62.	2.1	39
80	Effects of reclamation and natural changes on coastal wetlands bordering China's Yellow Sea from 1984 to 2015. Land Degradation and Development, 2019, 30, 1533-1544.	3.9	38
81	Quantifying the response of surface urban heat island to urbanization using the annual temperature cycle model. Geoscience Frontiers, 2022, 13, 101141.	8.4	38
82	Spatial, temporal, and spectral variations in albedo due to vegetation changes in China's grasslands. ISPRS Journal of Photogrammetry and Remote Sensing, 2019, 152, 1-12.	11.1	37
83	Optimizing Feature Selection of Individual Crop Types for Improved Crop Mapping. Remote Sensing, 2020, 12, 162.	4.0	37
84	Integrating remote sensing and geospatial big data for urban land use mapping: A review. International Journal of Applied Earth Observation and Geoinformation, 2021, 103, 102514.	2.8	37
85	Underestimates of Grassland Gross Primary Production in MODIS Standard Products. Remote Sensing, 2018, 10, 1771.	4.0	36
86	Evapotranspiration-dominated biogeophysical warming effect of urbanization in the Beijing-Tianjin-Hebei region, China. Climate Dynamics, 2019, 52, 1231-1245.	3.8	36
87	Mapping Forest and Their Spatial–Temporal Changes From 2007 to 2015 in Tropical Hainan Island by Integrating ALOS/ALOS-2 L-Band SAR and Landsat Optical Images. IEEE Journal of Selected Topics in Applied Earth Observations and Remote Sensing, 2018, 11, 852-867.	4.9	35
88	Long term trend and interannual variability of land carbon uptake—the attribution and processes. Environmental Research Letters, 2017, 12, 014018.	5.2	34
89	Impacts of ecological restoration projects on agricultural productivity in China. Journal of Chinese Geography, 2013, 23, 404-416.	3.9	33
90	A carbon monitoring system for mapping regional, annual aboveground biomass across the northwestern USA. Environmental Research Letters, 2020, 15, 095003.	5.2	32

#	Article	IF	CITATIONS
91	Different Patterns in Daytime and Nighttime Thermal Effects of Urbanization in Beijing-Tianjin-Hebei Urban Agglomeration. Remote Sensing, 2017, 9, 121.	4.0	31
92	Temporal consistency between gross primary production and solar-induced chlorophyll fluorescence in the ten most populous megacity areas over years. Scientific Reports, 2017, 7, 14963.	3.3	30
93	Expansion dynamics of deciduous rubber plantations in Xishuangbanna, China during 2000–2010. GIScience and Remote Sensing, 2018, 55, 905-925.	5.9	30
94	Effects of in-situ and reanalysis climate data on estimation of cropland gross primary production using the Vegetation Photosynthesis Model. Agricultural and Forest Meteorology, 2015, 213, 240-250.	4.8	29
95	Spatial–Temporal Changes of Water Resources in a Typical Semiarid Basin of North China over the Past 50 Years and Assessment of Possible Natural and Socioeconomic Causes. Journal of Hydrometeorology, 2013, 14, 1009-1034.	1.9	28
96	Continuous land cover change monitoring in the remote sensing big data era. Science China Earth Sciences, 2017, 60, 2223-2224.	5.2	27
97	Comparison of Pixel- and Object-Based Approaches in Phenology-Based Rubber Plantation Mapping in Fragmented Landscapes. Remote Sensing, 2018, 10, 44.	4.0	26
98	Accuracy Assessment and Inter-Comparison of Eight Medium Resolution Forest Products on the Loess Plateau, China. ISPRS International Journal of Geo-Information, 2017, 6, 152.	2.9	25
99	Identifying Establishment Year and Pre-Conversion Land Cover of Rubber Plantations on Hainan Island, China Using Landsat Data during 1987–2015. Remote Sensing, 2018, 10, 1240.	4.0	25
100	Examining rice distribution and cropping intensity in a mixed single- and double-cropping region in South China using all available Sentinel 1/2 images. International Journal of Applied Earth Observation and Geoinformation, 2021, 101, 102351.	2.8	25
101	Reply to Wang et al.: Snow cover and air temperature affect the rate of changes in spring phenology in the Tibetan Plateau. Proceedings of the National Academy of Sciences of the United States of America, 2013, 110, E2856-7.	7.1	24
102	Accelerating Cities in an Unsustainable Landscape: Urban Expansion and Cropland Occupation in China, 1990–2030. Sustainability, 2019, 11, 2283.	3.2	24
103	Quantifying the accuracies of six 30-m cropland datasets over China: A comparison and evaluation analysis. Computers and Electronics in Agriculture, 2022, 197, 106946.	7.7	24
104	Semi-natural areas of Tarim Basin in northwest China: Linkage to desertification. Science of the Total Environment, 2016, 573, 178-188.	8.0	22
105	Mapping Annual Forest Cover in Sub-Humid and Semi-Arid Regions through Analysis of Landsat and PALSAR Imagery. Remote Sensing, 2016, 8, 933.	4.0	21
106	Biophysical effects of paddy rice expansion on land surface temperature in Northeastern Asia. Agricultural and Forest Meteorology, 2022, 315, 108820.	4.8	21
107	Rapid surface water expansion due to increasing artificial reservoirs and aquaculture ponds in North China Plain. Journal of Hydrology, 2022, 608, 127637.	5.4	21
108	Are There Sufficient Landsat Observations for Retrospective and Continuous Monitoring of Land Cover Changes in China?. Remote Sensing, 2019, 11, 1808.	4.0	20

#	Article	IF	CITATIONS
109	Human Activities Enhance Radiation Forcing through Surface Albedo Associated with Vegetation in Beijing. Remote Sensing, 2020, 12, 837.	4.0	20
110	Mapping 20 years of irrigated croplands in China using MODIS and statistics and existing irrigation products. Scientific Data, 2022, 9, .	5.3	20
111	Canopy and climate controls of gross primary production of Mediterranean-type deciduous and evergreen oak savannas. Agricultural and Forest Meteorology, 2016, 226-227, 132-147.	4.8	19
112	Climate change affecting temperature and aridity zones: a case study in Eastern Inner Mongolia, China from 1960–2008. Theoretical and Applied Climatology, 2013, 113, 561-572.	2.8	18
113	Variations of Vegetation Phenology Extracted from Remote Sensing Data over the Tibetan Plateau Hinterland during 2000–2014. Journal of Meteorological Research, 2020, 34, 786-797.	2.4	17
114	Forest Changes by Precipitation Zones in Northern China after the Three-North Shelterbelt Forest Program in China. Remote Sensing, 2021, 13, 543.	4.0	17
115	Tracking spatiotemporal dynamics of irrigated croplands in China from 2000 to 2019 through the synergy of remote sensing, statistics, and historical irrigation datasets. Agricultural Water Management, 2022, 263, 107458.	5.6	17
116	Trends and variation in vegetation greenness related to geographic controls in middle and eastern Inner Mongolia, China. Environmental Earth Sciences, 2011, 62, 245-256.	2.7	14
117	Tracking Reforestation in the Loess Plateau, China after the "Grain for Green―Project through Integrating PALSAR and Landsat Imagery. Remote Sensing, 2019, 11, 2685.	4.0	14
118	Satellite evidence on the trade-offs of the food-water–air quality nexus over the breadbasket of India. Global Environmental Change, 2021, 71, 102394.	7.8	14
119	Annual 30-m big Lake Maps of the Tibetan Plateau in 1991–2018. Scientific Data, 2022, 9, 164.	5.3	14
120	Divergent changes in cropping patterns and their effects on grain production under different agro-ecosystems over high latitudes in China. Science of the Total Environment, 2019, 659, 314-325.	8.0	13
121	Warming Effort and Energy Budget Difference of Various Human Land Use Intensity: Case Study of Beijing, China. Land, 2020, 9, 280.	2.9	13
122	Reply to Shen et al.: No evidence to show nongrowing season NDVI affects spring phenology trend in the Tibetan Plateau over the last decade. Proceedings of the National Academy of Sciences of the United States of America, 2013, 110, E2330-1.	7.1	12
123	Elevation-dependent effects of growing season length on carbon sequestration in Xizang Plateau grassland. Ecological Indicators, 2020, 110, 105880.	6.3	12
124	Decision-Level and Feature-Level Integration of Remote Sensing and Geospatial Big Data for Urban Land Use Mapping. Remote Sensing, 2021, 13, 1579.	4.0	12
125	Non-uniform seasonal warming regulates vegetation greening and atmospheric CO <sub>2</sub> amplification over northern lands. Environmental Research Letters, 2018, 13, 124008.	5.2	11
126	The relationships between urban-rural temperature difference and vegetation in eight cities of the Great Plains. Frontiers of Earth Science, 2019, 13, 290-302.	2.1	11

#	Article	IF	CITATIONS
127	Assessing albedo dynamics and its environmental controls of grasslands over the Tibetan Plateau. Agricultural and Forest Meteorology, 2021, 307, 108479.	4.8	11
128	Multi-scale assessments of forest fragmentation in China. Biodiversity Science, 2017, 25, 372-381.	0.6	11
129	Integrated Analyses of PALSAR and Landsat Imagery Reveal More Agroforests in a Typical Agricultural Production Region, North China Plain. Remote Sensing, 2018, 10, 1323.	4.0	10
130	Improving Dengue Forecasts by Using Geospatial Big Data Analysis in Google Earth Engine and the Historical Dengue Information-Aided Long Short Term Memory Modeling. Biology, 2022, 11, 169.	2.8	10
131	Mismatches between vegetation greening and primary productivity trends in South Asia – A satellite evidence. International Journal of Applied Earth Observation and Geoinformation, 2021, 104, 102561.	2.8	9
132	Assessment of changes in the state of the rangelands of Inner Mongolia, China between 1998 and 2007 using remotely sensed data. Rangeland Journal, 2012, 34, 103.	0.9	8
133	Land Cover Change Intensifies Actual and Potential Radiative Forcing through CO2 in South and Southeast Asia from 1992 to 2015. International Journal of Environmental Research and Public Health, 2019, 16, 2460.	2.6	8
134	Understanding Current and Future Fragmentation Dynamics of Urban Forest Cover in the Nanjing Laoshan Region of Jiangsu, China. Remote Sensing, 2020, 12, 155.	4.0	8
135	Human activities modulate greening patterns: a case study for southern Xinjiang in China based on long time series analysis. Environmental Research Letters, 2022, 17, 044012.	5.2	8
136	Effectiveness in protected areas at resisting development pressures in China. Applied Geography, 2022, 141, 102682.	3.7	8
137	Gross Primary Production of Terrestrial Vegetation. Springer Remote Sensing/photogrammetry, 2014, , 127-148.	0.4	6
138	Monitoring tidal flats boundaries through combining Sentinel-1 and Sentinel-2 imagery. Environmental Technology and Innovation, 2021, 22, 101401.	6.1	6
139	Patterns and causes of winter wheat and summer maize rotation area change over the North China Plain. Environmental Research Letters, 2022, 17, 044056.	5.2	4
140	Suggestive Data Annotation for CNN-Based Building Footprint Mapping Based on Deep Active Learning and Landscape Metrics. Remote Sensing, 2022, 14, 3147.	4.0	3
141	Mapping irrigated croplands in China using a synergetic training sample generating method, machine learning classifier, and Google Earth Engine. International Journal of Applied Earth Observation and Geoinformation, 2022, 112, 102888.	1.9	3
142	Physical and Economic Processes of Ecosystem Services Flows. Physics and Chemistry of the Earth, 2017, 101, 1-2.	2.9	2
143	Mapping Panax Notoginseng Plantations by Using an Integrated Pixel- and Object-Based (IPOB) Approach and ZY-3 Imagery. Remote Sensing, 2021, 13, 2184.	4.0	2
144	Modeling urban sprawl effects on regional warming in Beijing-Tianjing-Tangshan urban agglomeration. Acta Ecologica Sinica, 2015, 35, .	0.1	2

#	Article	IF	CITATIONS
145	Community Composition and Structure Affect Ecosystem and Canopy Water Use Efficiency Across Three Typical Alpine Ecosystems. Frontiers in Plant Science, 2021, 12, 771424.	3.6	2
146	A robust but straightforward phenology-based ginger mapping algorithm by using unique phenology features, and time-series Sentinel-2 images. Computers and Electronics in Agriculture, 2022, 198, 107066.	7.7	2
147	Evaluating Effects of Medium-Resolution Optical Data Availability on Phenology-Based Rice Mapping in China. Remote Sensing, 2022, 14, 3134.	4.0	2
148	A spatial cluster method for prime farmland selection. Proceedings of SPIE, 2007, , .	0.8	1
149	Reply to: "Correlation between paddy rice growth and satellite-observed methane column abundance does not imply causation― Nature Communications, 2021, 12, 1189.	12.8	1
150	A Novel Approach for Automatic Urban Surface Water Mapping with Land Surface Temperature (AUSWM). Remote Sensing, 2022, 14, 3060.	4.0	1
151	VALERIE PELLEGRINO AVENI, Study abroad and second language use: Constructing the self. Language in Society, 2007, 36, .	0.5	0